Transmittance of Single Wall Carbon Nanotubes

W. Holmes,* J. Hone,† P. L. Richards, and A. Zettl

Physics Department,

University of California,

Berkeley, CA 94720

and

Materials Sciences Division,

Lawrence Berkeley National Laboratory,

Berkeley, CA 94720

(Dated: July 30, 2001)

Abstract

We have measured the far infrared absorption of single wall carbon nanotube (SWNT) ropes at 1.5K and SWNT ropes in polyethylene (PE) over the range $1.5 < T < 300K$. A weak peak is observed at $28cm^{-1}$ at 1.5K for free standing SWNT samples. The frequency and temperature dependence of the peak is consistent with absorption by an E_{2g} symmetric, "squash mode", SWNT phonon, which is infrared active due to an adsorbate or disorder. The peak frequency for SWNT ropes in PE is at $40cm^{-1}$ and temperature dependent. We attribute the increase in the frequency of the peak for SWNT in PE to the effect of $\approx 0.2GPa$ of hydrostatic pressure exerted on the SWNT ropes due to the thermal contraction of PE when cooled to low temperatures. Using two independent methods, we estimate that the SWNT may radially buckle at this pressure. The buckling distortion may cause the pressure dependence of the peak frequency. We cannot rule out the possibility that the peak is an absorption onset from adsorbate modes extrinsic to the SWNT or from interband transitions at a small electronic band gap. An effective medium calculation of Drude metal grains in polyethylene gives a frequency dependence consistent with our data, but the model underestimates the strength of scattering by orders of magnitude.

PACS numbers: 61.48.+c, 78.30.Na, 78.66.Tr, 63.22.+m

I. INTRODUCTION

Single wall carbon nanotubes (SWNT) are tubes of carbon tens of atomic diameters in circumference and $> 10^6$ atomic diameters long.[1–3] Several interesting properties have been measured on both mats of SWNT ropes and individual SWNT including a very high Young's modulus,[4,5] non-linear IV characteristics,[6–9] very high field emission from the tips,[10] quantum dot-like electronic confinement,[11,12] one dimensional (1D) phonon thermal conductance[13] and 1D heat capacity.[14] Phonon structure has been studied theoretically[15–20] and experimentally using Raman scattering.[20–26] Very few infrared measurements of SWNT have been reported.[22,27] We have measured the far infrared (FIR) transmittance of assemblages of single walled carbon nanotubes. These measurements probe excitations in the SWNT bundles at meV energies and electronic properties without problems associated with electrical contact.

II. SAMPLE PREPARATION

The SWNT ropes studied were provided by R. E. Smalley's group at Rice University. Details of the growth method are discussed elsewhere.[3] The chirality of the SWNT is described by an index pair (n, m). SWNT with $n = m$, or armchair tubes, are metals. With few exceptions, the others are semiconductors.[28] The measured diameter of the SWNT, $d = 1.37 \pm 0.04nm$, specifies the structure to a subset of indicies (n, m) *i.e.* (10,10),(18,0),(12,3).[28] During growth, the SWNT of different chiralities[26,29,30] form ropes consisting of ≈ 100 tubes arranged in a triangular lattice. The ropes of SWNT are removed from the growth chamber as a tangled mat. Transport measurements on individual tubes have shown both metallic and semiconducting behavior.[9,11,12]

We have prepared three types of samples for our FIR studies: as-grown mats ground up and dispersed in polyethylene (PE), as-grown mats, and mats treated to remove residue from the growth process. Samples of SWNT dispersed in PE were prepared for several reasons. Dispersion of the SWNT in the PE permitted the preparation of samples with larger transmittance without concern for light leaks than was possible for the mat samples. This improved the measurement accuracy at the high frequency end of our range. Also, the PE provided a higher thermal conductance to the SWNT grains than for mat samples. This enabled accurate measurement of the sample temperature in our evacuated apparatus.

The SWNT in PE samples were prepared as follows. A small section of a mat sample was put in medium density PE powder[32] in an aluminum dish and heated just above the 100°C melting point of PE. The mixture was repeatedly melted and ground, using a file, until uniformly black. The tube/PE mixture was melted once more and poured into $5mm$ diameter, $12mm$ long holes in brass sample mounts. The volume filling fraction of SWNT was determined to be $f = 5 \times 10^{-5}$ using the densities and measured weights of SWNT and PE. A slice of a sample was removed from the brass holder, melted, and viewed under a microscope. The grain size was measured to be $a \approx 1\mu m$. Several pure PE samples were prepared for normalization. We did not observe any bubbles in the PE which would produce additional scattering. Washers with $3.2mm$ diameter holes were glued to the SWNT/PE and PE sample mounts to prevent leakage of infrared around the edges when the samples contract upon cooling.

For the other two types of samples, layers were peeled from a large mat and laid across a $3mm$ diameter hole in a brass sample mount. A washer was glued over the edges of the mat to secure it in place and to prevent infrared leakage. The layers were $\approx 0.5mm$ thick and opaque when viewed by eye through the hole. Mat sample 1 was measured as grown without any further processing. Mat samples 2 and 3 were baked for 1 hour at $\approx 1200K$ in an Ar atmosphere to remove amorphous carbon residue left in the mats during growth. Mat sample 4 was prepared by placing SWNT mats in a solution of 30% HNO_3 in an ultrasonic bath, rinsing with distilled water, and filtering the solution through a porous carbonate substrate.[31] Mat samples 2, 3, and 4 contain $> 99\%$ SWNT ropes. The measured DC transport for all of the mat samples as a function of temperature is qualitatively similar.[7]

III. TRANSMITTANCE MEASUREMENT

The transmittance spectra were measured by Fourier transform spectroscopy with a resolution of $1.17cm^{-1}$. The step-and-integrate, Michelson interferometer was evacuated to a pressure of $< 30mTorr$ to avoid water vapor absorption and to increase the power output. An evacuated sample cryostat, shown in Figure 1, was used for transmittance measurements as a function of temperature. The samples were placed on a three position slider in a gap in the light pipe inside the evacuated cryostat. The slider was in good thermal contact with a cold finger which was cooled using flowing liquid helium. Coarse temperature regulation of

the cold finger was achieved by adjusting the flow of helium. Fine temperature regulation, $\approx 1\%$, was achieved using a commercial controller[33] at a series of fixed temperatures from $12 < T_s < 300K$. The FIR transmitted through the sample passed into a section of light pipe leading out of the sample cryostat and into the filter and detector apparatus shown in Figure 2. Cold low pass filters were mounted in the upper, 6 hole, rotating wheel to minimize background radiation on the detector and to define the spectral band so as to prevent aliasing. The bolometric detector was mounted in an evacuated can below the rotating wheels. Bolometers were optimized for different background power levels. The optical power was modulated at $20Hz$ and the detector output was demodulated using a lock-in amplifier. A sample of SWNT in PE, a sample of pure PE for normalization, and an empty sample holder were mounted in the slider. A spectrum of each sample was measured at each temperature point.

The apparatus, shown in Figure 2, was used for measurements of samples immersed in superfluid helium at $1.5K$. Samples were mounted on the lower wheel. One sample space was left blank to measure the output spectrum of the interferometer.

Transmittance was measured over the frequency range $10 - 100cm^{-1}$ and temperatures between 1.5K and 310K for samples of SWNT in PE. Representative transmittance measurements, shown in Figure 1, were achieved by averaging several two-minute scans. The absorption coefficients of the PE normalization samples and the samples of SWNT in PE were computed from

$$\alpha = \frac{-1}{t} \ln(\frac{T(\nu)}{1 - R_s}), \tag{1}$$

where t is the sample thickness and $T(\nu)$ is measured transmittance. The surface reflectance of pure PE, $R_s = 0.042$, is used for all calculations.[34] The Fabry-Perot fringes, with spacing $1/2nt \approx 0.27cm^{-1}$, are not resolved. The measured temperature dependent absorption coefficient of the PE, α_{PE}, is in excellent agreement with previous work.[35,36]

The absorption coefficient, α_{SWNT}, of a sample of SWNT in PE, with α_{PE} subtracted, is shown in Figure 3 for representative temperatures. All features in $\alpha_{SWNT} - \alpha_{PE}$ are weak. Features present in the SWNT in PE data are reproducible on thermal cycling from 1.5 - 314K, and are not present in the pure PE sample. There is a weak peak centered at $\approx 40cm^{-1}$ ($\approx 5meV$) which is temperature dependent.

The transmittance of mat samples at $1.5K$ ranged from 10^{-3} to 10^{-1} for the different thicknesses. Transmittance data for the mat samples cannot be expressed as an absorp-

tion coefficient, α, because the sample thickness is poorly defined. In Figure 4, they are presented as $-\log(Transmittance)$, which is proportional to α. They are multiplied by an arbitrary factor to compensate for different thicknesses so as to allow easy comparison of data for different mat samples. Effects due to surface reflection and diffuse scattering are not removed. Any resonant effects due to the geometry, similiar to those for inductive wire grid mesh filters, should occur outside our frequency range since the spacing between cross linking of the SWNT bundles in the as-grown mat samples is less than $1\mu m$. Samples 2-4 were all treated to remove amorphous carbon impurities and sample 1 was not. Sample 4, compared with samples 1-3, has more than an order of magnitude fewer impurities, is two orders of magnitude thinner, and should have a qualitatively different cross-linking pattern because it was filtered through the carbonate. In these data, we focus attention on a weak feature marked "peak." This peak could be the same as the small peak observed in the SWNT in PE samples, but shifted to lower frequencies due to the absense of hydrostatic pressure exerted on the SWNT from the thermal contraction of the PE.

It is convienient to express α in terms of the dielectric function, ϵ, and magnetic permeability μ,

$$\alpha = 4\pi\nu Im\sqrt{\epsilon\mu}. \tag{2}$$

We set $\mu = 1$ for most of this discussion. Using Equation 2, we calculate values of $\mathrm{Im}\sqrt{\epsilon} < 0.01$ from the absorption data for both pure PE and SWNT in PE. Since the real part of the index of refraction, $\mathrm{n} = \mathrm{Re}\sqrt{\epsilon} \approx 1.52$ is much larger than $\mathrm{Im}\sqrt{\epsilon} < 0.01$, R_s of SWNT in PE does not differ substantially from that of pure PE.

IV. FAR INFRARED ABSORPTION PEAK

There are four possible explanations of this peak based on published work. Explanations are discussed in an order corresponding to the size of their contribution to the heat capacity at low temperatures $< 50K$ since these measurements also probe meV excitation.[14] The first explanation is absorption by a low frequency, $\mathrm{E_{2g}}$ symmetric, optical phonon, of individual SWNT,[17,20] which might be infrared active due to adsorbed helium.[37] Here, the adsorbate provides oscillator strength to activate a mode instrinsic to the SWNT, but the adsorbate does not oscillate. Orientational disorder and inhomogeniety of SWNT chirality in the rope could also cause infrared activation of the $\mathrm{E_{2g}}$ mode of the SWNT in the rope. The second

explanation is absorption by molecular-like modes of the adsorbed molecules oscillating at the binding sites. These modes are extrinsic to the SWNT. The third and fourth explanations are absorption onset at an electronic band gap[38,39] or a librational mode of the SWNT in the rope lattice called a "twiston."[40,41]

The optical phonons and the band structure of SWNT are one-dimensional (1D) in nature. Therefore, the joint density of states diverges $D_{cv} \propto (hc\nu - E_b)^{-1/2}$, where E_b is the phonon or band gap energy.[28] The imaginary part of the dielectric function is

$$\mathrm{Im}(\epsilon) = \frac{e^2}{\epsilon_o c m^2} D_{cv}(hc\nu)|P_{cv}|^2, \tag{3}$$

where e is the electron charge, m is the reduced or effective mass, and ϵ_o is the permeability of free space. The transition matrix element, $|P_{cv}|^2$, for electronic transitions is usually weakly dependent on frequency.[42] For infrared active phonons, including the extrinsic adsorbate modes and twiston mode, $|P_{cv}|^2$ also peaks at E_b. Therefore, all explanations discussed above should cause a peak in α at $\nu_l = E_b/hc$. The absorption peak should be temperature dependent and most prominent below $\sim 50K$ where the thermal energy is sufficiently below the excitation energy $hc\nu$.

Low frequency, zone center, 1D optical phonon modes in SWNT result from quantization of the circumferential wave vector or, analogously, "band-folding" of the two dimensional graphene sheet phonon dispersion relation. The low temperature heat capacity of SWNT ropes is dominated by contributions from the 1D acoustic and optical phonons.[14] The lowest energy optical phonon is a Raman active, E_{2g} symmetric, mode which is characterized by a squashing or flattening of opposing sides of the tube.[17] This so-called "squash mode" is not infrared active in SWNT ropes or isolated SWNT, but could be activated by adsorbed molecules or orientational disorder of the SWNT in the rope.[39,43] Adsorbed molecules cause Raman active and silent modes to become infrared active in similar forms of carbon such as C_{60} and C_{70}.[37] The peak in the FIR absorption is weak as expected for a mode that is not infrared active in the SWNT rope without adsorbate or disorder.

Hone *et al.* demonstrate that the heat capacity is strongly enhanced at $T_s < 20K$ by adsorbed helium.[14] The temperature dependence of the intensity of the FIR absorption peak could be due to desorption of helium from the SWNT ropes. At low temperatures, $T_s < 20K$, helium is adsorbed and the phonon modes are infrared active. At temperatures $20 < T_s < 55K$, the helium begins to desorb and the strength of the far infrared absorption

decreases. At $T_s \gg 55K$, the helium is completely desorbed and no peak is expected, consistent with the FIR data.

Weak absorption in the FIR by low energy phonons is well known in disordered materials, such as fused quartz. The disorder breaks translational and rotational symmetry so infrared absorption is allowed without conservation of wave vector. The temperature dependence of the absorption peak, if infrared active due to disorder, can be described by orientational melting.[43] In SWNT ropes at low temepratures, rotational disorder in the rope lattice is fixed and the phonon is infrared active. At higher temperatures, the thermal energy exceeds the weak binding energy that fixes the rotation of the SWNT in the rope and the individual SWNT rachet among equivalent equillibrium sites. If the period of motion of the SWNT over equivalent sites in the rope lattice is much shorter than the period of the phonon mode $\approx 1ps$ then the effect of the disorder on the infrared activation is reduced and the absorption peak decreases. This so called orientational melting temperature, T_{OM}, of SWNT[43] is predicted at $T_{OM} \approx 160K$, slightly higher than the temperature, $\approx 55K$, at which the absorption peak disappears in our FIR data. A similar orientational melting describes the temperature dependence of absorption by a phonon in C_{60} and C_{70}.[37]

Hone *et al.* [14] find the frequency of the squash mode for $1.25nm$ diameter tubes in a nanorope is $34cm^{-1}$ from analysis of their heat capacity data. The squash mode phonon frequency scales as $1/d^2$.[20] By this scaling argument, we expect that the phonon frequency is $28cm^{-1}$ in our $d = 1.37nm$ SWNT rope samples. The agreement with the measured peak frequency, at $\approx 28cm^{-1}$ in all the bare mat samples of SWNT ropes, is remarkable.

The calculated frequency of the squash mode for a lone SWNT is $\approx 20cm^{-1}$.[16,17,20] From a tight binding calculation, which includes the effect of intertube coupling, Kahn and Lu predict the squash mode frequency is $41cm^{-1}$ for (10,10) type of $d = 1.37nm$ SWNT in a rope.[17] Numerical analysis of the heat capacity data indicates that the intertube coupling used in theoretical calculations is at least a factor 5 too large for $1.25nm$ SWNT ropes. If the peak is the squash mode and since the measured peak frequency is in between the values for lone SWNT and the SWNT in a rope, our data would support the conclusion from the analysis of the heat capacity data.[14]

The aspect of the data that is not clearly supported by the literature is the difference in the peak frequency $\approx 40cm^{-1}$ for the SWNT ropes dispersed in PE and cooled to $1.5K$ compared to the peak frequency in the mat samples $\approx 28cm^{-1}$. The PE contracts due

$\delta l/l \approx 4\%$ on cooling.[44] The majority of the contraction occurs between 300 and $100K$. It is reasonable to assume that the thermal contraction of the SWNT is negligble in comparsion. This differential thermal contraction causes pressure on the SWNT ropes at the interface with the PE. The pressure, P, exerted by the PE on the SWNT is

$$P \approx \frac{B_{PE}\delta l/l}{1 + B_{PE}/B_t}. \tag{4}$$

We fix the total strain at 4% and assume that the pressure is uniform at the interface. The bulk modulus of the PE[44] is $B_{PE} \approx 5GPa$. The calculated bulk modulus of the SWNT ropes is $B_t \approx 25GPa$.[45] A smaller value of $B_t \approx E_r \approx 8GPa$, may be more accurate for the following reason. Shen *et al.* measured the elastic modulus for radial compression, E_r, by pressing on the sides of $10nm$ diameter multiwalled carbon nanotubes (MWNT).[46] They found that E_r is a factor ~ 100 smaller than the axial elastic modulus, E_a, inferred from bending.[47] If this were true of SWNT in a rope, then $E_r \approx 8 \pm 4GPa$, where we have divided E_a measured in bending[4] or by axial strain[5] by 100. Plugging B_{PE} and B_t into Equation 4, we estimate $0.1 - 0.2GPa$ of hydrostatic pressure is exerted on the SWNT ropes in the PE at temperatures $< 100K$. Theoretical calculations[17] correctly predict the measured pressure dependence of the A_{1g} symmetric, radial breathing mode for $d = 1.73nm$ SWNT at $\approx 186cm^{-1}$,[21,25] and the tangential mode quadruplet at $1549 - 1600cm^{-1}$[24,25] below pressures $\approx 1.5GPa$. The calculated increase in the frequency of the squash mode at 0.2 GPa of hydrostatic pressure is $\approx 6cm^{-1}$,[17] which is a factor 2 smaller than the measured shift of $\approx 12cm^{-1}$.

The shift could be due to radial buckling of SWNT in the rope when under hydrostatic pressure in the PE at low temperatures. If the SWNT buckled radially, the shape of the SWNT and forces between SWNT in the rope would be dramatically different than those used in the calculations. This could explain the disagreement with our measured shift. Venkateswaran *et al.* tentatively assign the observation of a complete loss of Raman scattering cross section of the of the A_{1g} symmetric, radial breathing mode at a pressure of 1.5GPa to the onset of a hexagonal deformation of the SWNT in the rope.[25] This type of pressure induced change of the SWNT is the microscopic analog of radial buckling of a macroscopic tube. The critical pressure, p_{crit}, for radial buckling of a thin wall, macroscopic tube is[48]

$$p_{crit} = \frac{2(k^2 - 1)E_r t^3}{d^3(1 - \mu_P^2)}, \tag{5}$$

where distorted tube cross sections, perpendicular to the tube length, for various values of $k = 1, 2, \cdots$ are shown in Figure 5. At p_{crit} with $k = 2$, for example, the SWNT, with a circular cross section, is in an unstable equillibrium with a flattened shape. The buckling distortion for $k = 2$ is the same form as the distortion for the squash mode. Therefore, the squash mode should be strongly affected once p_{crit} for $k = 2$ is exceeded. A value of $p_{crit} = 0.13GPa$ is obtained for the $k = 2$ distortion when scaled from the hexagonal distortion, $k = 6$ using Equation 5. An independent confirmation of this value of $p_{crit} = 0.13GPa$ for $k = 2$ is obtained using the elastic modulus for radial compression $E_r = 8GPa \pm 4GPa$ inferred from experimental data,[4,5,46] the measured tube diameter, $d = 1.37nm$, wall thickness $t \approx 0.34nm$ used by other authors,[5,49] and the Poisson ratio calculated for an individual SWNT,[45,50] $\mu_P \approx 0.3$. Plugging these values into Equation 5 with $k = 2$ the estimated value of $p_{crit} = 0.28 \pm 0.14GPa$. This is consistent with the scaling argument and comparable to the pressure applied to the SWNT in the PE.

Our absorption peak does not disappear at or above the buckling distortion as did the intensity of Raman scattering due to the breathing mode.[25] Ventkateswaran *et al.* postulate that the hexagonal distortion shifts peaks in the electronic density of states near the Fermi level, which dramatically reduces the resonant enhancement of the Raman scattering of the 2.41 eV photon energy used for their measurements.[21,25] Either mechanism proposed to cause the FIR absorption peak is not expected to depend as sharply on pressure.

Another severe deformation is rearrangement of the SWNT in the rope at high pressure. In this case, the pressure shears the SWNT in the cylindrical lattice rope which causes the SWNT to slip into an elliptical lattice. The shear modulus of SWNT rope is known to be small $\approx 1GPa$.[49] Other mechanisms such as coupling of the polyethylene to the SWNT or differences in intercolation of helium into the bare mat samples compared to the SWNT rope in PE samples could cause the frequency of the peak to increase.

A small electronic band gap could cause the absorption peak in our FIR data. This mechanism, or any other electronic excitation, would not contribute significantly to the heat capacity since the 1D phonon contributions in SWNT are always larger.[14] The peak in the bare mat samples, shown in Figure 4, is at $28cm^{-1}$, or equivalently a photon energy of 3.5meV. Electronic band gaps are predicted at the Fermi level in SWNT of $\approx 3-5meV$ which result from carbon-carbon bond-stretching relative to the graphene sheet.[38] A "pseudogap" is also predicted at the Fermi level, caused by intertube interactions of SWNT in a rope, but at

higher energies.[39,51] The frequency and temperature dependence of the measured absorption are consistent with the presence of an electronic band gap in the samples of SWNT ropes. The absorption is higher for photon energies larger than the gap energy since valence band electrons are excited into the conduction band. At temperatures $T_s > E_b/k = 40K$, the peak in α is reduced significantly since electrons thermally populate the conduction band and fill the states at the conduction band edge. Also, the electron density, measured by Hall effect on samples of $d = 1.37nm$ SWNT ropes from the same batch,[7] increases at $T_s > 40K$, consistent with thermal excitation of electrons into the conduction band.

The pressure dependence of the peak is not that expected for an electronic band gap. The band gap should scale[38] $E_b \propto 1/d^2$. Our best estimate of the strain on the SWNT is $< 1\%$. Therefore the expected increase in the band gap of the SWNT in PE $< 1cm^{-1}$ or $< 0.1meV$ is nearly an order of magnitude smaller than the measured increase. The strong pressure dependence could be explained by an extreme distortion of the SWNT, such as radial buckling.

It has been noted that the frequency of the peak absorption is close to predicted values of the frequency of the librational mode of SWNT in the rope called a "twiston."[51] Analysis of the measured heat capacity[14] sets an upper limit for the twiston mode frequency of $< 5cm^{-1}$, well below the predicted values which lie in the range $12 - 50cm^{-1}$.[40,41,51] Using this analysis, we rule out the interpretation of the peak as due to absorption by twiston modes. The signal to noise ratio in our apparatus was not sufficient to determine if a mode existed at frequencies $< 5cm^{-1}$.

Measuring the FIR transmittance of the SWNT ropes as a function temperature with various adsorbates is key to differentiating models for the peak in absorption. Transmittance measurements of SWNT in a vacuum for example, using a procedure similar to that of Hone *et al.* which removes the adsorbed helium, would verify whether adsorbed helium causes infrared activation of the squash mode or if the peak is due to adsorbate modes extrinsic to the SWNT. If the absorption peak does not depend on adsorbates, then it is probably orientational disorder that causes the squash mode phonon to be infrared active. Measurement of the small Raman shift corresponding to the squash mode would discriminate whether the absorption peak is caused by an electronic band gap.

V. SCATTERING DUE TO FREE ELECTRONS IN BUNDLES OF SWNT

We use the effective medium theory[52] to model the absorption of SWNT in PE. Effective medium theory has been used in other studies of nanotubes in different ways. Bommeli *et al.* use the effective medium theory in the analysis of infrared spectra of multiwalled nanotubes to remove the effects of carbon and metal residues remaining from the growth process.[53] Garcia-Vidal *et al.* use effective medium theory to analyze the electromagnetic fields at an individual tube within an array of other tubes when the wavelength is comparable to the tube diameter.[54] Their analysis explains measured SWNT response at energies $3.0 < h c \nu < 7.0$eV.[55]

We approximate the SWNT bundles as a simple metal with the Drude dielectric function

$$\epsilon_m = \epsilon_\infty - \frac{\omega_p^2}{\omega^2 + i\omega/\tau}, \tag{6}$$

where ε_∞ is the static dielectric function at high frequency, $\omega_p = 2\pi c \nu_p$, and c is the speed of light. It is useful to express the DC conductivity, $\sigma = \omega_p^2 \tau \varepsilon_0$, in terms of the plasma frequency and the scattering rate.

Using this model dielectric function for the SWNT bundles, we write the dielectric function for the effective medium in the Maxwell-Garnet approximation, where the filling fractions of the SWNT grains is $f \ll 1$,[52]

$$\epsilon_{EMT} = \epsilon_{PE} + 3 f \epsilon_{PE} \frac{\epsilon_m - \epsilon_{PE}}{(1-f)(\epsilon_m - \epsilon_{PE}) + 3\epsilon_{PE}}. \tag{7}$$

Here, ϵ_{PE} is the complex dielectric function of the PE host.

The main qualitative difference between absorption in a bulk metal and the grains in the effective medium is the magnetic coupling to the grains. The magnetic permeability is significant when the penetration depth, δ, is much greater than the particle size, $\delta \gg a$. In large particles, $\delta \ll a$, the magnetic field can only penetrate a small fraction of the volume. However, if this same volume of material is ground into particles with sizes $\delta \gg a$, the magnetic field penetrates all of the material and leads to higher absorptivity. The magnetic polarizability of the grains can be written

$$\gamma_m \approx \frac{3}{8\pi}\left(\frac{3}{(ka)^2} - 1 - \frac{3}{ka}\cot(ka)\right), \tag{8}$$

where $k = 2\pi\nu\sqrt{\epsilon_m}$.[56]

The effective magnetic permeability, due entirely to the enhanced response of the SWNT grains, is

$$\mu_{EMT} = \frac{1 + f\frac{8\pi}{3}\gamma_m}{1 - f\frac{4\pi}{3}\gamma_m}, \tag{9}$$

in the limit of small f. Using the effective response functions from the model, ϵ_{EMT} and μ_{EMT}, the absorption coefficient is

$$\alpha_{EMT} = 4\pi\nu\,\mathrm{Im}(\sqrt{\epsilon_{EMT}\mu_{EMT}}), \tag{10}$$

where ν is the frequency in cm^{-1}. Treating the grains as cylindrical particles and averaging over the particle orientation is equivalent to treating the grains as spheres.

In the dirty limit, $\omega\tau \ll 1$, the Drude dielectric function simplifies to $\epsilon_m = \epsilon_\infty + \omega_p^2\tau/\omega$. Then the response ratio of the effective medium is

$$\frac{\alpha_{EMT}}{\alpha_{PE}} \approx [1 + f\nu(\frac{k_1}{\omega_p^2\tau} + k_2 a^2\omega_p^2\tau)], \tag{11}$$

where k_1 and k_2 are constants of order unity. Note that the response ratio, α_{EMT}/α_{PE}, depends linearly on frequency.

In the clean limit, $\omega\tau \gg 1$, the Drude dielectric function simplifies to $\epsilon_m = \epsilon_\infty - \omega_p^2/\omega^2$. An estimate of the carrier density for the nanotubes is $n > 10^{-19}cm^{-3}$. The corresponding plasma frequency is $\omega_p > 1000cm^{-1}$. For graphite, the value of $\epsilon_\infty \approx 2$, so ϵ_m simplifies even further to $\epsilon_m = -\omega_p^2/\omega^2$. The expression for ϵ_{EMT} simplifies from

$$\epsilon_{EMT} \approx \epsilon_{PE} + 3f\epsilon_{PE}\frac{\epsilon_\infty - \epsilon_{PE} - \omega_p^2/\omega^2}{\epsilon_\infty + 2\epsilon_{PE} - \omega_p^2/\omega^2}, \tag{12}$$

to $\epsilon_{EMT} = (1 - 3f)\epsilon_{PE}$. The magnetic permeability is a function of $k = 2\pi\nu\sqrt{\epsilon_m} = \omega_p$, which is constant in the clean limit. Therefore, the response ratio of the effective medium is constant,

$$\frac{\alpha_{EMT}}{\alpha_{PE}} = \sqrt{\mu_{EMT}}. \tag{13}$$

To summarize, the limiting behavior of the effective medium in the dirty limit is $\alpha_{EMT}/\alpha_{PE} \approx 1 + f\nu \times$ constant, and for the clean limit is $\alpha_{EMT}/\alpha_{PE} \approx$ constant.

The absorption coefficient of the SWNT in PE over the entire range of temperatures measured is shown in Figure 6. Using any reasonable set of parameters our model underestimates the absorption coefficient of the SWNT by orders of magnitude. In our model,

the absorption coefficient is dominated by direct absorption in the SWNT grains. We therefore conclude that neglected effects, such as adsorbed molecules on the surface or elastic scattering from the SWNT grains, dominate the measured absorption coefficients. Order of magnitude estimates of the absorption coefficient calculated using elastic scattering theory are consistent with our data. The electronic properties of the SWNT, in principle, could be obtained from fitting our data using expressions for scattering from cylindrical particles,[57] or by using the calculated density of states and a quantum partial wave scattering analysis.

VI. CONCLUSIONS

We have measured the transmittance of ropes of $d = 1.37nm$ SWNT prepared in different ways at 1.5K and the temperature dependence of SWNT in PE from $1.5 < T_s < 300$. There is a weak peak in the measured transmittance spectrum of SWNT ropes in PE at $40cm^{-1}$ at 1.5K and also in bare SWNT rope samples at $28cm^{-1}$ at 1.5K and zero pressure. The peak disappears at $T_s > 55K$. The peak could be absorption by the "squash mode" phonon which is infrared active due to the presence of adsorbed helium or other adsorbate(s) or due to disorder of the SWNT in the rope. Similar behavior has been observed in C_{60} and C_{70} .[37] The measured frequency of the peak is in excellent agreement with the value of the squash mode frequency determined from the heat capacity. The temperature dependence of the peak can be described by desorption of helium in the temperature range 20-55K[14] or by orientational melting.[43] We attribute the increase in the peak frequency for the SWNT in PE of $12cm^{-1}$ higher than measured for the bare mat samples to hydrostatic pressure applied to the SWNT ropes by thermal contraction of the PE when cooled to cryogenic temperatures. We estimate that the SWNT in the PE are under $\approx 0.2GPa$ of hydrostatic pressure. The dependence of squash mode frequency, if linear with pressure, is $\approx 60cm^{-1}/GPa$ which is stronger than predicted by theory.[17] The two independent methods we used to estimate the critical pressure[48] for a flattening distortion of the SWNT, $k = 2$ in Equation 5, predict a value in the range $p_{crit} \approx 0.1 - 0.2GPa$. We propose that the flattening distortion causes the frequency of the squash mode to depend on pressure more strongly than predicted by theory.[17] We cannot eliminate the possibility that the peak is an absorption onset from adsorbate modes extrinsic to the SWNT. Measurements of the FIR transmittance of SWNT ropes in vacuum, treated to remove the adsorbed helium after Hone *et al.* , and for different adsorbates are key to

understanding the role of adsorbates. FIR transmittance measurements may prove to be a useful tool to study adsorbates in SWNT structures. The absorption could be due to inter-band transitions at a small, carbon-carbon bond-stretching type of electronic energy gap.[38] A "pseudogap" is also predicted in the electronic band structure of SWNT ropes, but at an order of magnitude higher energy.[39,51] The heat capacity is necessarily dominated by contributions from the 1D SWNT phonons at low temperatures and therefore cannot be used to discriminate causes of the peak in our data. Measurements using a different technique, such as Raman scattering, are required to address these possibilities. Interpretation of the peak as an absorption onset from a librational phonon ("twiston") mode in SWNT ropes is inconsistent with the heat capacity measured for ropes of $d = 1.25nm$ SWNT.[14] Therefore, we do not favor twistons as a possible cause of the absorption peak. We have modeled the broadband absorption of SWNT grains in PE using the effective medium theory. This model underestimates the absorption. We conclude that the measured absorption coefficients are dominated by elastic scattering from the SWNT grains.

VII. ACKNOWLEDGEMENTS

We thank R. E. Smalley for providing the laser-vaporization-prepared nanotube samples used in this study and R. Mallozzi and J. Orenstein for assistance with preliminary measurements. This work was supported in part by the Director, Office of Science, Office of Basic Energy Sciences of the U.S. Department of Energy under Contract No. DE-AC03-76SF00098. J. H. acknowledges support from the U.S. Department of Education.

REFERENCES

* Permanent Address: MS79/24, Jet Propulsion Laboratory, Pasadena, CA 91109

† Permanent Address: Condensed Matter Physics, California Institute of Technology 114-36, Pasadena, CA 91125

[1] S. Iijima, Nature **354**, 56 (1991).

[2] D. Bethune, C. Kiang, M. deVries, G. Gorman, R. Savoy, J. Vazquez, and R. Beyers, Nature **363**, 605 (1993).

[3] A. Thess, R. Lee, P. Nikolaev, H. Dai, P. Petit, J. Robert, C. Xu, Y. Lee, S. G. Kim, A. Rinzler, D. Colbert, G. Scuseria, *et al.*, Science **273**, 483 (1996).

[4] N. Chopra, *Structure and Elastic Properties of Nanotubes*, Ph.D. thesis, University of California, Berkeley (1996).

[5] M.-F. Yu, B. S. Files, S. Arepalli, and R. S. Ruoff, Phys. Rev. Lett. **84**, 5552 (2000).

[6] P. G. Collins, A. Zettl, H. Bando, A. Thess, and R. Smalley, Science **278**, 100 (1997).

[7] M. Fuhrer, U. Varadarajan, W. Holmes, P. Delaney, S. Louie, and A. Zettl, in *Proceedings of the IWEPNM*, edited by H. Kuzmany (Euro. Phys. Soc., Vienna, Austria, 1998), pp. 123–30.

[8] P. Kim, T. W. Odom, J.-L. Huang, and C. M. Lieber, Phys. Rev. Lett. **82**, 1225 (1999).

[9] M. S. Fuhrer, J. Nygå rd, L. Shih, M. Forero, Y.-G. Yoon, M. Mazzoni, H. J. Choi, J. Ihm, S. G. Louie, A. Zettl, and P. L. McEuen, Science **288**, 494 (2000).

[10] P. Collins and A. Zettl, Appl. Phys. Lett. **69**, 1969 (1996).

[11] M. Bockrath, D. Cobden, P. McEuen, N. Chopra, A. Zettl, A. Thess, and R. Smalley, Science **275**, 1922 (1997).

[12] S. Tans, M. Devoret, H. Dai, A. Thess, R. Smalley, L. Georliga, and C. Dekker, Nature **386**, 474 (1997).

[13] J. Hone, M. Whitney, C. Piskoti, and A. Zettl, Phys. Rev. B **59**, R2514 (1999).

[14] J. Hone, B. Batlogg, Z. Benes, A. Johnson, and J. Fischer, Science **289**, 1730 (2000).

[15] J. Yu, R. Kalia, and P. Vashishta, J. Chem. Phys. **103** (1995).

[16] R. Saito, T. Takeya, T. Kimura, G. Dresselhaus, and M. Dresselhaus, Phys. Rev. B **57**, 4145 (1998).

[17] D. Kahn and J. P. Lu, Phys. Rev. B **60**, 6535 (1999).

[18] T. Maeda and C. Horie, Physica B **263-264**, 479 (1999).

[19] V. Sokhan, D. Nicholson, and N. Quirke, J. Chem. Phys. **113**, 2007 (2000).

[20] M. Dresselhaus and P. Eklund, Adv. Phys. **49**, 705 (2000).

[21] G. Rao, E. Richter, S. Bandow, B. Chase, P. Eklund, W. Williams, S. Fang, K. Subbaswamy, M. Menon, A. Thess, R. Smalley, G. Dresselhaus, *et al.*, Science **275**, 187 (1997).

[22] J. Kastner, T. Pichler, H. Kuzmany, S. Curran, *et al.*, Chem. Phys. Lett. **221**, 53 (1994).

[23] A. Kasuya, Y. Sasaki, Y. Saito, K. Tohji, and Y. Nishina, Phys. Rev. Lett. **78**(23), 4434 (1997).

[24] A. Jorio, G. Dresselhaus, M. Dresselhaus, M. Souza, M. Dantas, M. Pimenta, A. Rao, R. Saito, C. Liu, and H. Cheng, Phys. Rev. Lett. **85**, 2617 (2000).

[25] U. Venkateswaran, A. Rao, E. Richter, M. Menon, A. Rinzler, R. Smalley, and P. Eklund, Phys. Rev. B **59**, 10928 (1999).

[26] A. Jorio, R. Saito, J. Hafner, C. Lieber, M. Hunter, T. McClure, G. Dresselhaus, and M. Dresselhaus, Phys. Rev. Lett. **86**, 1118 (2001).

[27] A. Kuznetsova, D. B. Mawhinney, V. Naumenko, J. T. Yates Jr, J. Liu, and R. Smalley, Chem. Phys. Lett. **321**, 292 (2000).

[28] M. Dresselhaus, G. Dresselhaus, and R. Saito, Carbon **33**, 883 (1995).

[29] T. Odom, H. Jin-Lin, P. Kim, and C. Lieber, Nature **391**, 62 (1998).

[30] J. Wildoer, L. Venema, A. Rinzler, R. Smalley, and C. Dekker, Nature **391**, 59 (1998).

[31] S. Bandow, A. Rao, K. Williams, A. Thess, R. Smalley, and P. Eklund, J. of Phys. Chem. B **101**, 8839 (1997).

[32] Medium Density Polyethylene Powder, Fischer Scientific, Fairlawn, NJ 07410.

[33] Lake Shore Cryotronics, Inc., 64 E. Walnut St., Westerville, OH 43081; Model GRT-200.

[34] J. Birch, J. Dromey, and J. Lesurf, Infrared Physics **21**, 225 (1981).

[35] J. Zirke and M. Meissner, Infrared Physics **18**, 871 (1978).

[36] W. Frank, H. Schmidt, and W. Wulff, J. Pol. Sci. **61**, 317 (1977).

[37] S. FitzGerald and A. Sievers, J. Chem. Phys. **101**, 7283 (1994).

[38] C. Kane and E. Mele, Phys. Rev. Lett. **78**, 1932 (1997).

[39] P. Delaney, H. Choi, J. Ihm, S. Louie, and M. Cohen, Nature **391**, 466 (1998).

[40] Y.-K. Kwon, D. Tománek, Y. Lee, K. Lee, and S. Saito, Phys. Rev. B **71**, 9887 (1997).

[41] A. Mizel, L. Benedict, M. Cohen, S. Louie, A. Zettl, N. Budraa, and W. Beyermann, Phys. Rev. B **60**, 3264 (1999).

[42] P. Y. Yu and M. Cardona, *Fundamentals of Semiconductors* (Springer Verlag, Heidelberg, Germany, 1996).

[43] Y.-K. Kwon and D. Tománek, Phys. Rev. Lett. **84**, 1483 (2000).

[44] I. Engeln, M. Meissner, and H. Pape, Polymer **26**, 364 (1985).

[45] J. Lu, Phys. Rev. Lett. **79**, 1297 (1997).

[46] W. Shen, B. Jiang, B. S. Han, and S.-s. Xie, Phys. Rev. Lett. **84**, 3634 (2000).

[47] M. Treacy, T. Ebbsen, and J. Gibson, Nature **381**, 678 (1996).

[48] J. Den Hartog, *Advanced Strength of Materials* (Dover, New York, 1987), 274-278.

[49] J.-P. Salvetat, G. A. D. Briggs, J.-M. Bonard, R. R. Bacsa, A. J. Kulic, T. Stöckli, N. A. Burnham, and L. Forró, Phys. Rev. Lett. **82**, 944 (1999).

[50] G. Zhou, W. Duan, and B. Gu, Chem. Phys. Lett. **333**, 344 (2001).

[51] Y.-K. Kwon, S. Saito, and D. Tománek, Phys. Rev. B **58**, R13314 (1998).

[52] G. L. Carr, S. Perkowitz, and D. B. Tanner, *Infrared and Millimeter Waves* (Academic Press, New York, 1985), chap. 6, pp. 171–263.

[53] F. Bommelli, L. Digiorgi, L. Forro, *et al.*, Solid State Comm. **99**, 513 (1996).

[54] F. Garcia-Vidal, J. Pitarke, and J. Pendry, Phys. Rev. Lett. **78**, 4289 (1997).

[55] W. de Heer *et al.*, Science **268**, 845 (1995).

[56] G. Ford and S. A. Werner, Phys. Rev. B **8**, 3702 (1973).

[57] G. van Hulst, *Light Scattering by Small Particles* (Dover, New York, 1981), 1st ed.

VIII. FIGURE CAPTIONS

FIG. 1: Representative measured transmittance as a function frequency of SWNT in PE on a semilog scale. The B_{1u} PE phonon is clear at 1.5K. The PE phonon has shifted to $73cm^{-1}$ and is much weaker at 300K. The signal to noise ratio is poor for transmittance $< 10^{-3}$. The cryostat used for measurement of temperature dependent transmittance is shown in the inset. The FIR enters at the top through a light pipe. Inside the cryostat, the light pipe sections (A and B) are attached to a cooled radiation baffle (C) which surrounds the sample slider (D) and cold finger (E). The coldfinger is cooled by flowing liquid ^{4}He . Thermometers (F and G) were attached to the slider and cold finger. A heater (H) on the cold finger was used to regulate the temperature. Three samples (J) are mounted on the slider, where the sliding direction is perpendicular to the plane of the page, and are interchanged while at each temperature set point.

FIG. 2: System used for measuring samples immersed in liquid helium at 1.5K. The FIR from the step-and-integrate Michelson interferometer with Hg-arc source passes through warm IR blocking filters and into the glass cryostat. The samples are mounted on a wheel in a gap near the bottom of the light pipe. Cold blocking filters are mounted both in a filter wheel above the samples and also below the samples at the entrance to the bolometer can. A Winston concentrator and a composite bolometer are located in an evacuated can sealed by a polypropylene window. The FIR is modulated at 20Hz inside the interferometer. The bolometer signal is demodulated with a lock-in amplifier, digitized, and Fourier transformed.

FIG. 3: The temperature dependence of $(\alpha_{SWNT} - \alpha_{PE})$ for SWNT in PE. The data for $\geq 23K$ have been offset by arbitrary factors for clarity. The arrow denotes the position of the "peak" discussed in the text.

FIG. 4: Measured frequency dependence of the negative log of the transmittance for mats of SWNT, samples 1-4, at 1.5K. The data have a resolution of $1.2cm^{-1}$ and are multiplied by an arbitrary factor to compensate for different thicknesses so as to allow easy comparison. All data have increasing log(Transmittance) with increasing frequency to a plateau in the range $10 < \nu < 20cm^{-1}$. At $\nu > 20cm^{-1}$, there is a broad peak for all samples at $\approx 28cm^{-1}$. Samples 1-3 have log(Transmittance) independent of frequency from $30 < \nu < 70cm^{-1}$. Sample 4 increases with ν in this range. Mat sample 4 is approximately two orders of magnitude thinner than samples 1-3 and was processed differently as described in the text.

FIG. 5: Cross sections of SWNT for the undeformed, flattened $k = 2$, and hexagonally distorted $k = 6$ cases (solid lines) under hydrostatic pressure. The undeformed cross section (dashed line) is superimposed on the distorted shapes for reference.

FIG. 6: The response ratio, $(\alpha_{SWNT}/\alpha_{PE} - 1)$, as a function of frequency on an expanded scale for the SWNT sample in PE. Each panel shows part of the temperature range. As the temperature is increased, the response ratio first decreases (a), then increases (b), and finally decreases (c). The values of α_{SWNT} and α_{PE} vary by more than one order of magnitude over the frequency range measured. However, the ratio is nearly constant at frequencies $> 30 cm^{-1}$.

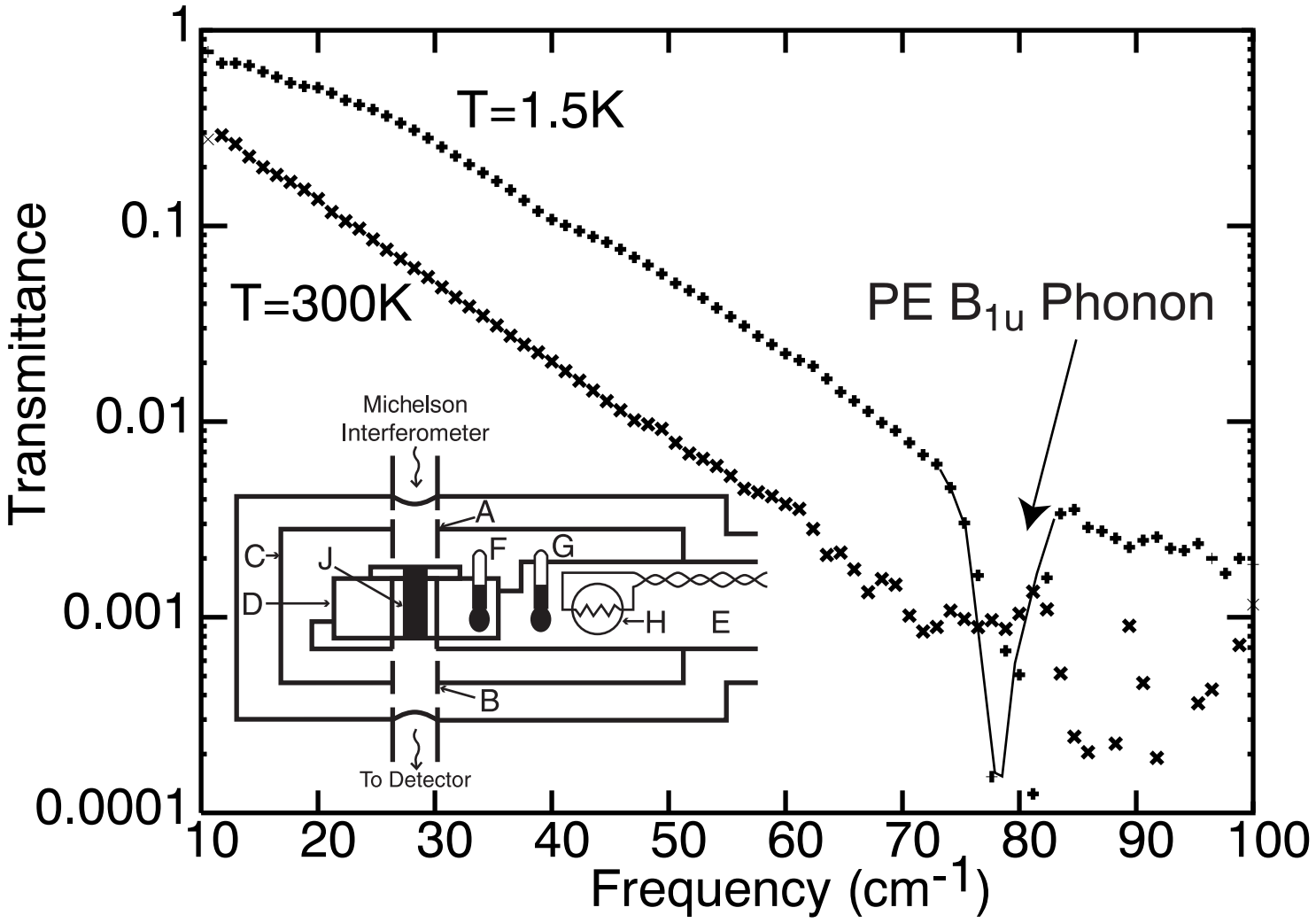
T=1.5K
T=300K
PE B_{1u} Phonon
Transmittance
Frequency (cm^{-1})
1
0.1
0.01
0.001
0.0001
10
20
30
40
50
60
70
80
90
100
Michelson
Interferometer
A
B
C
D
E
F
G
H
J
To Detector

Figure 1

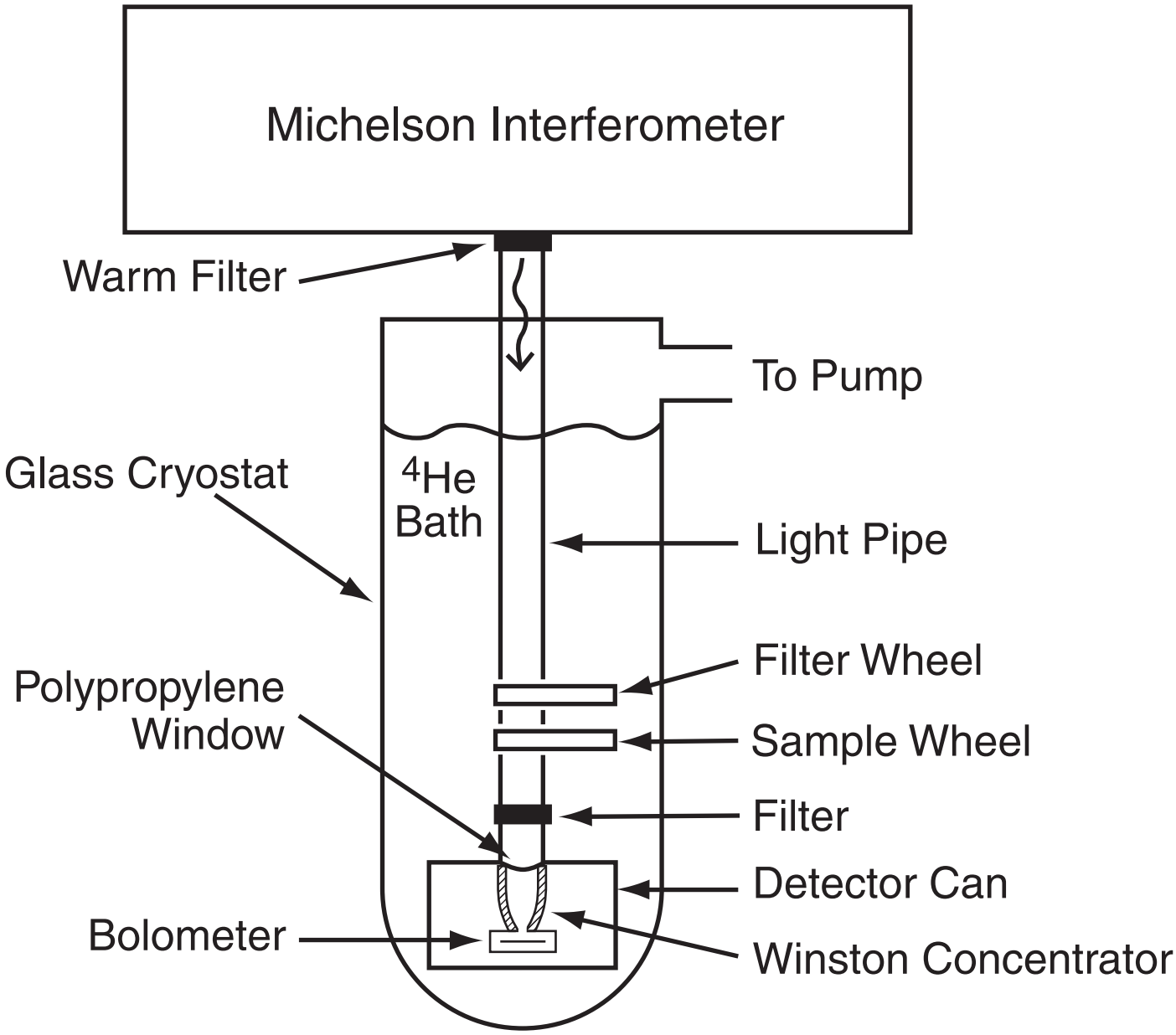
Michelson Interferometer
Warm Filter
To Pump
Glass Cryostat
^{4}He
Bath
Light Pipe
Filter Wheel
Polypropylene
Window
Sample Wheel
Filter
Detector Can
Bolometer
Winston Concentrator

Figure 2

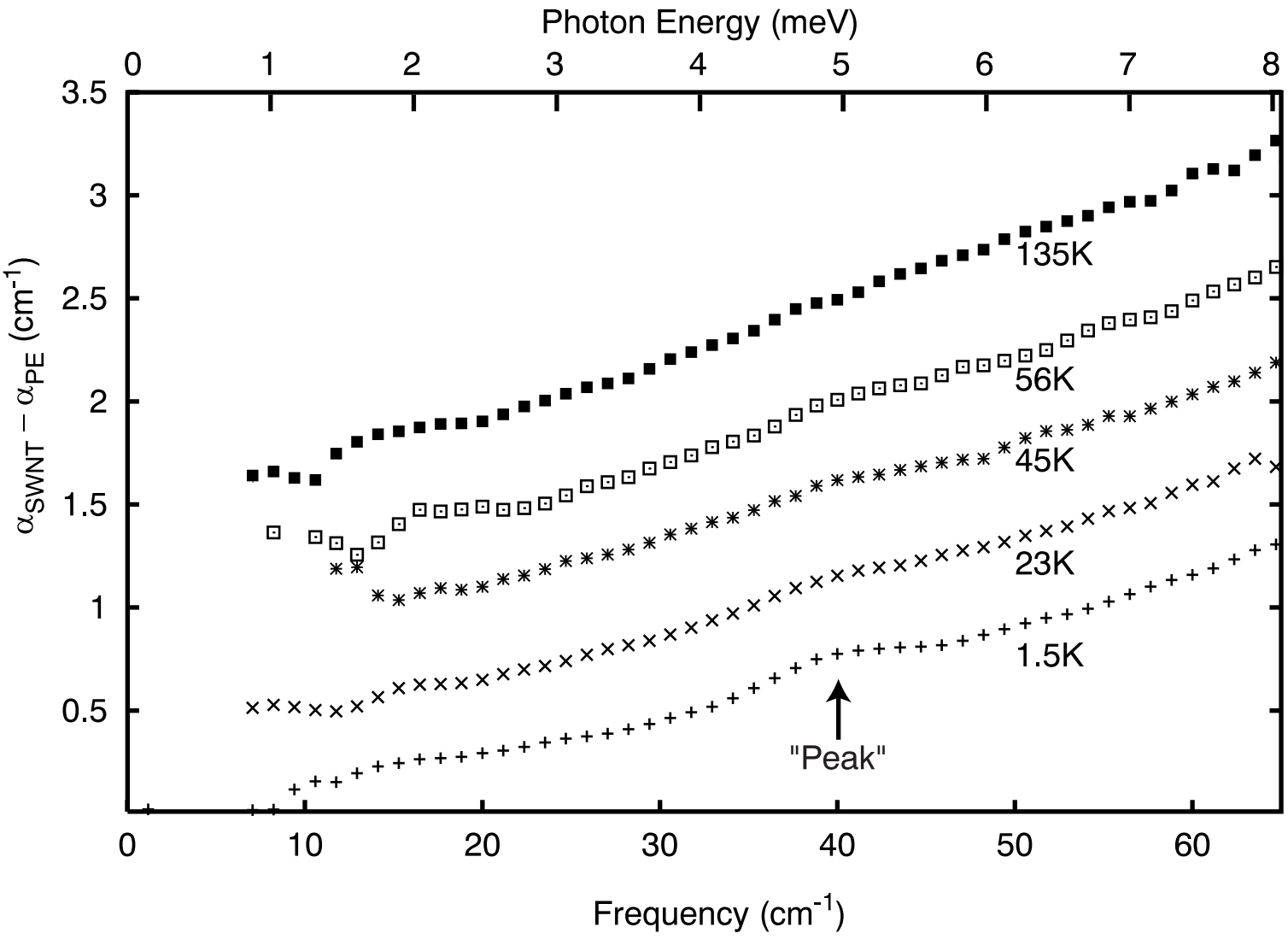
Photon Energy (meV)
0
1
2
3
4
5
6
7
8
3.5
3
2.5
2
1.5
1
0.5
$\alpha_{SWNT} - \alpha_{PE}$ (cm^{-1})
135K
56K
45K
23K
1.5K
"Peak"
0
10
20
30
40
50
60
Frequency (cm^{-1})

Figure 3

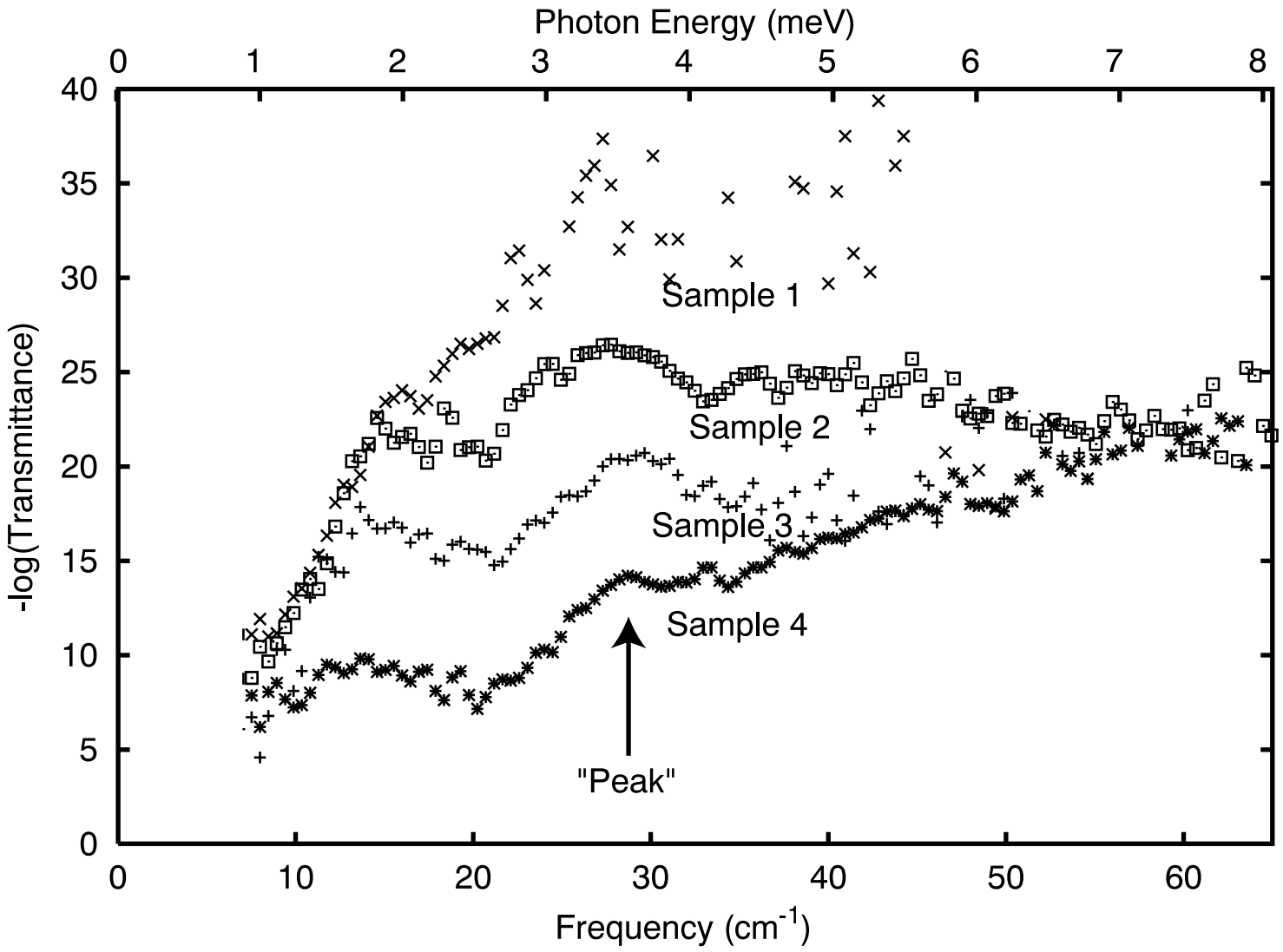
Photon Energy (meV)
0
1
2
3
4
5
6
7
8
-log(Transmittance)
40
35
30
25
20
15
10
5
0
Sample 1
Sample 2
Sample 3
Sample 4
"Peak"
0
10
20
30
40
50
60
Frequency (cm-1)

Figure 4

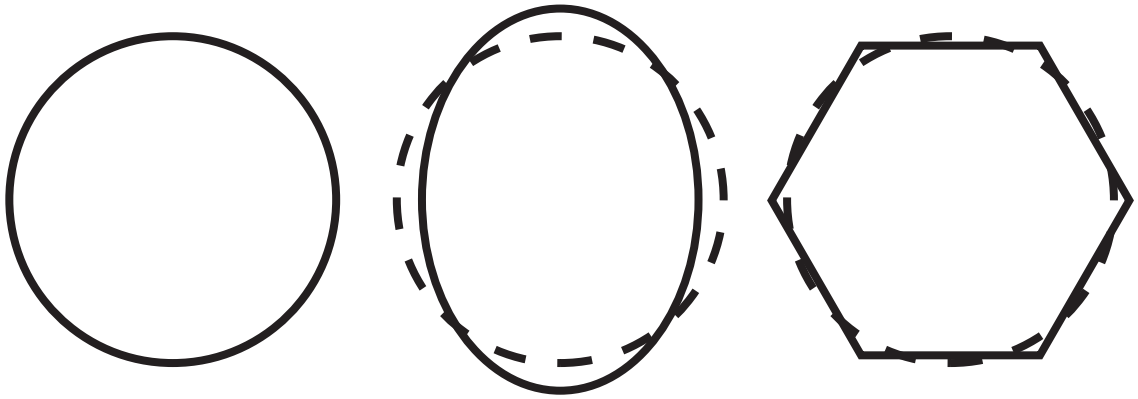

Figure 5

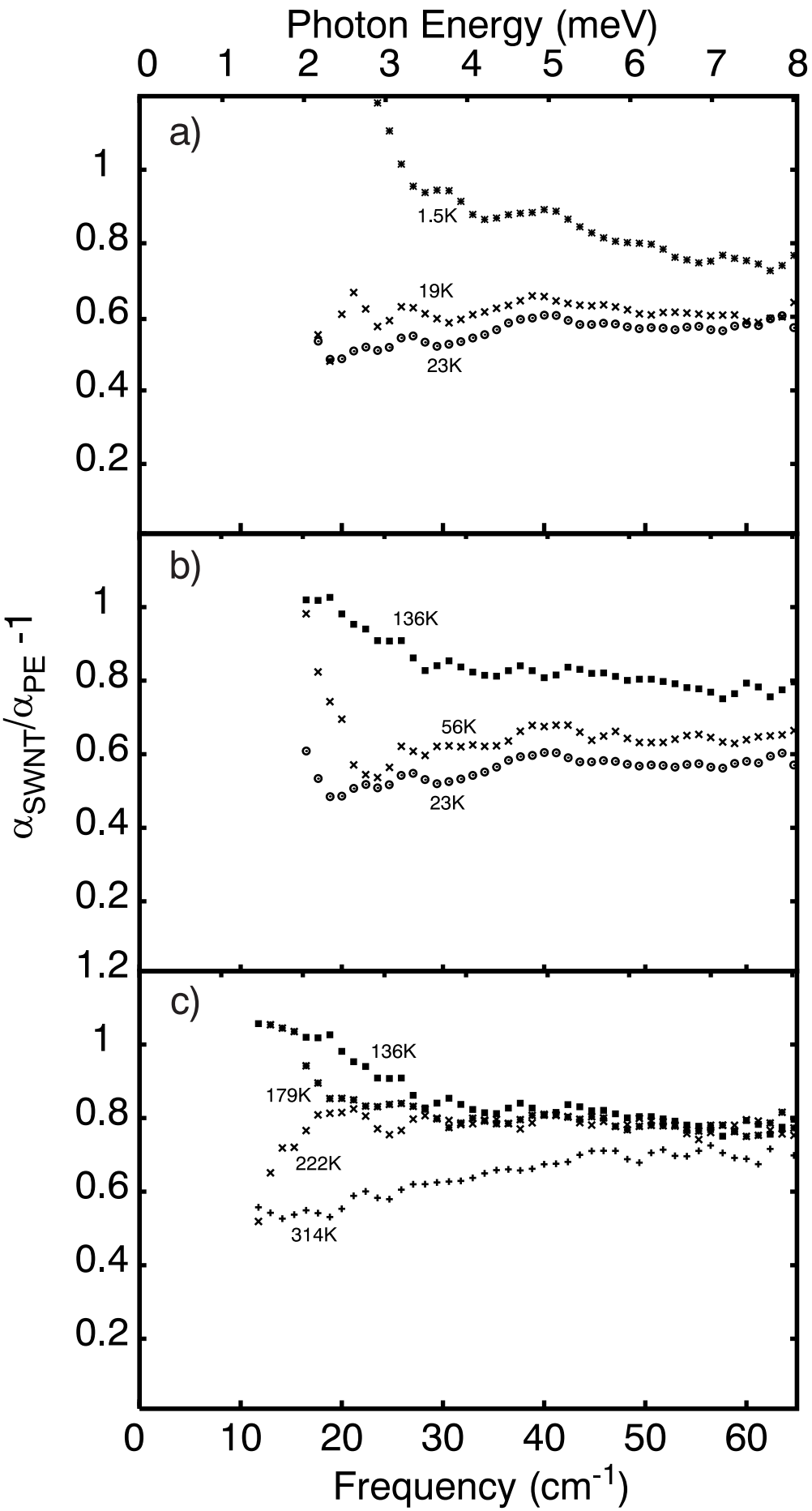
Photon Energy (meV)
0 1 2 3 4 5 6 7 8
a)
1.5K
19K
23K
b)
136K
56K
23K
c)
136K
179K
222K
314K
$\alpha_{SWNT}/\alpha_{PE}$ -1
0 10 20 30 40 50 60
Frequency (cm^{-1})

Figure 6